NJC

Accepted Manuscript

This is an *Accepted Manuscript*, which has been through the Royal Society of Chemistry peer review process and has been accepted for publication.

Accepted Manuscripts are published online shortly after acceptance, before technical editing, formatting and proof reading. Using this free service, authors can make their results available to the community, in citable form, before we publish the edited article. We will replace this *Accepted Manuscript* with the edited and formatted *Advance Article* as soon as it is available.

You can find more information about *Accepted Manuscripts* in the Information for Authors.

Please note that technical editing may introduce minor changes to the text and/or graphics, which may alter content. The journal's standard Terms & Conditions and the Ethical guidelines still apply. In no event shall the Royal Society of Chemistry be held responsible for any errors or omissions in this *Accepted Manuscript* or any consequences arising from the use of any information it contains.

ROYAL SOCIETY OF CHEMISTRY

www.rsc.org/njc

Journal Name

RSC Publishing

ARTICLE

Electrically conductive polyaniline sensitized defective-TiO_2 for improved visible light photocatalytic and photoelectrochemical performance: A synergistic effect

Cite this: DOI: 10.1039/x0xx00000x

Received 00th January 2012,
Accepted 00th January 2012

DOI: 10.1039/x0xx00000x

www.rsc.org/

Mohd Omaish Ansari,[a*] Mohammad Mansoob Khan,[b*] Sajid Ali Ansari,[a] and Moo Hwan Cho[a*]

Sulfonated polyaniline@pure-TiO_2 (*s*-Pani@*p*-TiO_2) and polyaniline@defective-TiO_2 (*s*-Pani@*m*-TiO_2) nanocomposites were prepared by the *in-situ* oxidative polymerization of aniline in the presence of TiO_2 (*p*-TiO_2 and *m*-TiO_2) nanoparticles followed by sulfonation with fuming sulfuric acid. Defect-induced TiO_2 (*m*-TiO_2) nanoparticles were obtained by an electron beam (EB) treatment of commercial TiO_2 (*p*-TiO_2) nanoparticles. The resulting *s*-Pani@*p*-TiO_2 and *s*-Pani@*m*-TiO_2 nanocomposites were characterized by UV-visible diffuse absorbance spectroscopy, photoluminescence spectroscopy, transmission electron microscopy, X-ray diffraction, and X-ray photoelectron spectroscopy. Polyaniline (Pani) was dispersed uniformly over the defective *m*-TiO_2 surface with intimate contact on the interface to act cooperatively with the defects introduced deliberately to achieve remarkably enhanced properties. The *s*-Pani@*m*-TiO_2 nanocomposite showed better photocatalytic activity and photoelectrochemical performance than *s*-Pani@*p*-TiO_2 under visible light irradiation, which was attributed partly to the sensitizing effect of Pani, the narrowed band gap of *m*-TiO_2 and the effective interfacial interaction between Pani and *m*-TiO_2. The electrical conductivity measured using a four-point probe revealed *s*-Pani@*m*-TiO_2 to have much higher conductivity than *s*-Pani@*p*-TiO_2. Therefore, *s*-Pani@*m*-TiO_2 may be used for a wide range of applications owing to its higher charge mobility and high photocatalytic activity. The proposed methodology can also be a potential route for the development of nanocomposites via EB treatment and can be commercialized.

Introduction

Nanocrystalline TiO_2 has attracted considerable attention as a prime photocatalyst material since Honda and Fujishima reported the photo-oxidation of water on TiO_2.[1] Afterwards, TiO_2 has been exploited widely for the photodegradation of organic pollutants in wastewater because of its exceptional optical properties, non-toxicity, low cost, and high stability towards photo and chemical corrosion.[2] On the other hand, the solar energy to hydrogen efficiency of TiO_2 is limited substantially by its wide band gap as well as the high rate of electron and hole recombination, and requires UV light excitation for the catalytic reactions.[3] To develop solar-driven/visible light active photocatalysts without the need for extra light sources, several approaches, such as the doping of dyes,[4] metal ions,[5] noble metals,[6] composite formation with polymers,[7] etc. have been adopted as effective modification methods to enhance its efficiency for visible light-induced photodegradation reaction systems. Most of these techniques, however, often require multiple synthetic routes as well as hazardous chemicals. Therefore, a simpler synthesis via a greener route is needed.

Recently, electron beam (EB) irradiation has been used to modify the molecular structure of metal oxides to tune their band gap.[8] The solvated electrons formed during EB irradiation are a strong reducing agent capable of reducing metal ions to different valence states, leading to the formation of a range of defects (low valent cation formation and/or oxygen vacancy) in the lattice structure, which opens a new field towards the defect-induced band gap narrowing of metal oxides.[9] X. Hou et al.[10,11] revealed the enhanced catalytic activity of EB-treated TiO_2 and Pt@TiO_2 compared to the pure one by successfully degrading methyl orange under visible light irradiation. Similar results of enhancing the photocatalytic activity of TiO_2 by changing its surface structure by EB irradiation have been reported.[12,13] Therefore, based on these observations, it is believed that the EB irradiation technique can be an excellent method to modify the molecular structure and tune the band gap of TiO_2.

In a previous report, metal oxides nanocomposite with polyaniline (Pani) were employed to achieve a greater absorption of light in the UV and visible region, which leads to the sensitization of metal oxides, because Pani acts as a light harvester and sensitizer for

New Journal of Chemistry Accepted Manuscript

metal oxides, such as TiO_2.[14] Therefore, because of the sensitization ability of Pani, it is believed that a composite of EB-modified TiO_2 with Pani will have unique properties, such as enhanced photocatalytic activity under visible region, high stability, etc., because of the synergism between the constituents.

In our previous report we successfully reduced the band gap of TiO_2 (*m*-TiO_2) by creating defects (Ti^{3+} and/or oxygen vacancies) using an EB. The XRD, UV-visible absorption spectra, electron paramagnetic resonance and XPS analysis clearly revealed the existence of defects in m-TiO_2.[15] In continuation to that, in this study, the reported highly visible light active EB-modified TiO_2 (*m*-TiO_2) photoctalyst was further used for the synthesis of Pani@*m*-TiO_2 nanocomposite by simple in-situ oxidative polymerization of aniline in the presence of *m*-TiO_2 under dilute polymerization conditions using a small volume of aniline. For comparison, the commercial TiO_2 (*p*-TiO_2) nanocomposite with Pani (Pani@*p*-TiO_2) was also prepared similarly. The resulting nanocomposites (Pani@*p*-TiO_2 and Pani@*m*-TiO_2) were sulfonated by fuming H_2SO_4 because of the greater stability of sulfonated Pani towards redox reactions, and are called *s*-Pani@*p*-TiO_2 and *s*-Pani@*m*-TiO_2 for sulfonated Pani@*p*-TiO_2 and Pani@*m*-TiO_2, respectively. The prepared nanocomposites were first characterized and studied to understand the interfacial interactions between Pani and TiO_2 (*m*-TiO_2 and *p*-TiO_2). Later, both the prepared nanocomposites were used for the photocatalytic degradation of methylene blue (MB) and brilliant blue (BB) dyes under visible light irradiation. The *s*-Pani@*m*-TiO_2 nanocomposite showed enhanced visible light photocatalytic activity and photoelectrochemical behavior compared to the *s*-Pani@*p*-TiO_2 nanocomposite. The electrical conductivity of *s*-Pani@*p*-TiO_2 and *s*-Pani@*m*-TiO_2 was also evaluated; the latter showed higher conductivity than *s*-Pani@*p*-TiO_2.

Experimental

Materials

Aniline, MB, BB, and TiO_2 (mean particle size ~21 nm) were purchased from Sigma Aldrich. Potassium persulphate (PPs), HCl, NH_4OH, H_2SO_4, and methanol were obtained from Duksan Pure Chemicals, Korea, and used as received. The de-ionized water used in these experiments was obtained from a PURE ROUP 30 water purification system.

Methods and studies

An EB accelerator (ELV-0.5, BINP, Russia) with a maximum beam power, maximum beam current and maximum beam energy of 28 kW, 40 mA and ~0.7 MeV, respectively, was used to modify *p*-TiO_2. X-ray diffraction (XRD, PANalytical, X'Pert-PRO MPD) was performed using Cu Kα radiation (λ = 0.15405 nm). The UV-visible diffuse absorbance and reflectance were measured using a UV-VIS-NIR spectrophotometer (VARIAN, Cary 5000 USA). The microstructures were observed by field emission transmission electron microscopy (FE-TEM, Tecnai G2 F20, FEI, USA). X-ray photoelectron spectroscopy (XPS, XPS, K-ALPHA) was performed using a monochromatized Al Kα X-ray source (hν = 1486.6 eV). The photocatalytic degradation and photoelectrochemical experiments, such as electrochemical impedance spectroscopy (EIS) and linear scan voltammetry (LSV), were conducted using a 400 W lamp with an irradiation intensity of 31.0 $mWcm^{-2}$ (3M, USA). Details of the photoelectrode preparation for photoelectrochemical measurements are reported elsewhere.[6] EIS and LSV were carried out using a potentiostat (Versa STAT 3, Princeton Research, USA) with a standard three-electrode system with Ag/AgCl (saturated with KCl), Pt gauge and *s*-Pani@*p*-TiO_2 or *s*-Pani@*m*-TiO_2 nanocomposites coated FTO glass as the reference, counter and working electrodes, respectively, in a 0.2 M Na_2SO_4 solution as the electrolyte. For each electrode, the photocurrent response was examined by LSV in the dark and under visible light irradiation at a scan rate of 50 mV/s over a potential range of -0.9 to +0.9 V. EIS was performed in the dark and later under visible light irradiation at 0.0 V and at frequencies ranging from 1 to 10^4 Hz.

All DC electrical conductivity (σ) measurements were performed using a 4-in-line probe electrical conductivity measuring instrument with a PID controlled oven (Scientific Equipments, Roorkee, India). The calculations were performed using the following equation:

$$\sigma = [\ln 2(2S/W)]/[2\pi S(V/I)] \quad (1)$$

where I, V, W, and S are the current (A), voltage (V), pellet thickness (cm), and probe spacing (cm), respectively, and σ is the DC electrical conductivity (S/cm).[14]

The electrical conductivity of the *s*-Pani@*p*-TiO_2 and *s*-Pani@*m*-TiO_2 nanocomposites were measured using pelletized samples on a hydraulic pressure instrument at a pressure of 50 kN for 10 min. The *s*-Pani@*p*-TiO_2 and *s*-Pani@*m*-TiO_2 nanocomposites were also tested for the photocatalytic degradation of MB and BB under visible light irradiation; details of the experimental setup are reported elsewhere.[7,14] Details of the photoelectrochemical measurements, such as EIS and LSV, can be obtained from a previous report.[7]

Synthesis of *s*-Pani@*p*-TiO_2 and *s*-Pani@*m*-TiO_2 nanocomposites

EB modification of the TiO_2 nanoparticles was achieved using a method reported elsewhere.[15] In a typical process, 100 mL of an aqueous dispersion of *p*-TiO_2 (50 mM) was prepared. Upon EB exposure, the color of the *p*-TiO_2 changed to light pale yellow. The resulting dispersion was centrifuged to isolate the yellowish-white *m*-TiO_2 nanoparticles, which were dried in an air oven at 100 °C for 12 h and then stored in a desiccator for further experiments.

The Pani@*m*-TiO_2 nanocomposite was synthesized by the simple in-situ oxidative polymerization of aniline in the presence of *m*-TiO_2 under dilute polymerization conditions using a small amount of aniline monomer. In a typical process, 0.25 mL of aniline monomer was added to 0.5 g of *m*-TiO_2 and stirred vigorously for 2 h for proper adsorption of the aniline monomer on *m*-TiO_2 nanoparticles followed by the addition of a solution of oxidant (PPs solution prepared in 1 M HCl) to affect the polymerization reaction. The reaction mixture transformed to a greenish-black slurry, which was filtered after 2 h, washed sequentially with distilled water and an excess of methanol to remove the dissolved impurities and Pani

New Journal of Chemistry Accepted Manuscript

 This journal is © The Royal Society of Chemistry 2012

oligomers. The nanocomposites were de-doped with 1 M NH_4OH and later sulfonated with fuming H_2SO_4, as reported elsewhere.[16] Subsequently, the prepared sulfonated *s*-Pani@*m*-TiO_2 nanocomposite was dried at 80 °C for 6 h in an air oven, converted to fine powders and stored in a desiccator for further experiments. The sulfonated, *s*-Pani@*p*-TiO_2 nanocomposite was also prepared similarly in the presence of the *p*-TiO_2 nanoparticles.

Results and discussion

Proposed synthesis mechanism

The EB irradiation process was employed for the modification of TiO_2 nanoparticles.[15] The modification process employed a simple and completely greener route compared to the tedious chemical methods adopted, which generally require harsh chemicals. This leads to the creation of defects, such as Ti^{3+} formation and/or oxygen vacancies in *m*-TiO_2, which can be exploited further to produce nanocomposites with Pani to give hitherto unreported properties. The synthesized *s*-Pani@*m*-TiO_2 nanocomposite was expected to show a strong electrical response and photocatalytic activity because Pani imparts its electrical conductivity and shows high absorbance in the visible region. Fig. 1 presents a schematic diagram of the synthesis of *s*-Pani@*p*-TiO_2 or *s*-Pani@*m*-TiO_2 nanocomposites.

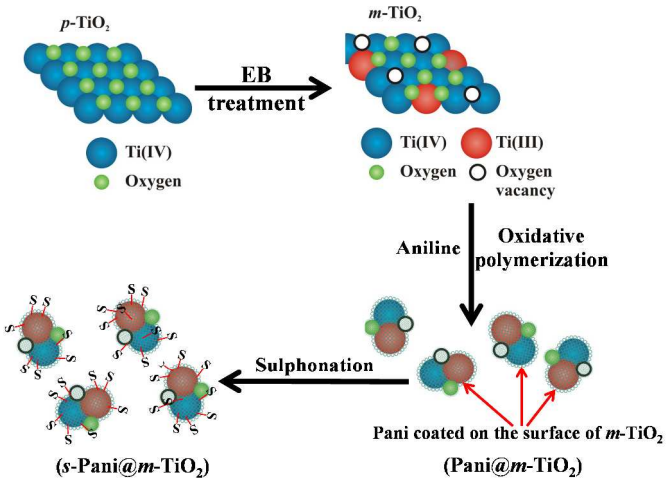

Fig. 1. Schematic diagram of the synthesis of the *s*-Pani@*m*-TiO_2 nanocomposite.

Structural analysis

Fig. 2 shows XRD patterns of *s*-Pani@*p*-TiO_2 and *s*-Pani@*m*-TiO_2 nanocomposites. In the case of *s*-Pani@*p*-TiO_2, sharp crystalline peaks (Fig. 2) for the anatase and rutile phases of TiO_2 were observed, which is similar to previous reports.[7,14] On the other hand, the characteristic peaks of Pani at ~15.1, 20.7 and 25.5 2θ° were not observed because of the small amount of aniline polymerized on the surface of the TiO_2 nanoparticles due to the dilute polymerization conditions.[17] The peaks for TiO_2 were indexed to their corresponding (hkl) parameters. Similar results were observed for the *s*-Pani@*m*-TiO_2 nanocomposite. On the other hand, *s*-Pani@*m*-TiO_2 compared to *s*-Pani@*p*-TiO_2 showed a slightly reduced peak intensity, which might be due to a change in the surface texture and defects in *m*-TiO_2.[15] This was also attributed to the interfacial interaction between Pani and *m*-TiO_2, which plays an important role in imparting novel characteristics to the *s*-Pani@*m*-TiO_2 nanocomposite. The crystallite size of TiO_2 in the *s*-Pani@*p*-TiO_2 and *s*-Pani@*m*-TiO_2 nanocomposites were calculated using the Scherrer's formula and the calculated crystallite size was 24.5 and 28.9 nm, respectively. This also corresponds to the TEM studies (Fig. 3). Overall, the crystallinity of the *s*-Pani@*p*-TiO_2 and *s*-Pani@*m*-TiO_2 nanocomposites was similar. Kim et al.[8] reported no significant changes in the intensity and peak position of TiO_2 after EB modification and concluded that the morphology and crystal structure of TiO_2 were not affected significantly by EB irradiation. Similar results were also reported by Hou et al.[11] in their Pt/TiO_2 thin films prepared by EB irradiation. In this case, a slight decrease in the crystallinity of *s*-Pani@*m*-TiO_2 was observed from which it can be concluded that EB irradiation alters the crystal structure of *p*-TiO_2 slightly with a decrease in the crystallinity of the TiO_2 nanoparticles by inducing defects in the crystal lattice, which also leads to lattice expansion.[15,18] In addition, the fine coating of *m*-TiO_2 by Pani might also be responsible for the decrease in the XRD peak intensity, which further proves the interfacial interaction between Pani and *m*-TiO_2.

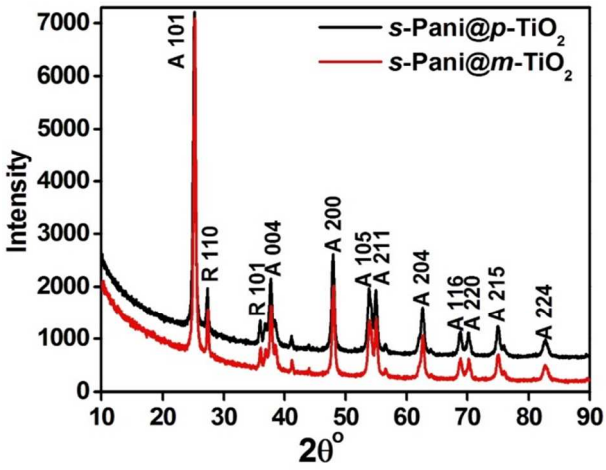

Fig. 2. XRD patterns of *s*-Pani@*p*-TiO_2 and *s*-Pani@*m*-TiO_2 nanocomposites.

Morphological studies

The morphology and inner nanostructure of the as-prepared *s*-Pani@*m*-TiO_2 nanocomposite was examined by TEM (Fig. 3). The particle size of the *s*-Pani@*m*-TiO_2 nanocomposite was ~20-30 nm, which corresponds to the XRD results. HR-TEM (Fig. 3b) revealed single TiO_2 crystals with a high degree of structural uniformity and a well-ordered lattice structure in both the inside and boundary, revealing a good level of crystallization. Fig. 3b also shows the interfacial interaction between Pani and *m*-TiO_2. The lattice spacing of 0.37 nm matched the distance between the (101) planes of the anatase TiO_2 crystal, which is also a prominent reflection peak in

New Journal of Chemistry Accepted Manuscript

XRD. The boundary shows that a thin, uniform and intact coating of Pani formed on the surface of *m*-TiO_2, which is responsible for the difference in the physical and chemical behavior of *m*-TiO_2 and *s*-Pani@*m*-TiO_2. The SAED pattern (Inset in Fig. 3a) also showed a distinct diffraction maximum and the sequential appearance of dark and bright fringes, which are the characteristic of the polycrystalline structures of the *s*-Pani@*m*-TiO_2 nanocomposite.

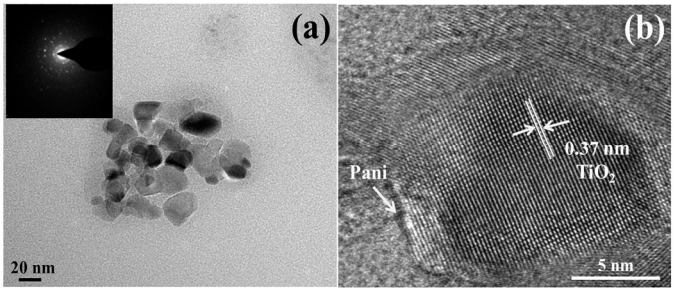

Fig. 3. (**a**) TEM and (**b**) HR-TEM images of the *s*-Pani@*m*-TiO_2 nanocomposite.

Compositional analysis

XPS was conducted for composition and surface analysis of the *s*-Pani@*p*-TiO_2 and *s*-Pani@*m*-TiO_2 nanocomposites (Fig. 4). The survey XP spectrum in Fig. S1a revealed the existence of Ti, O, C, and N in the *s*-Pani@*p*-TiO_2 and *s*-Pani@*m*-TiO_2 nanocomposites. The peak in Fig. S1b (C 1s = 285.17 eV for *s*-Pani@*p*-TiO_2 and 284.75 for *s*-Pani@*m*-TiO_2) was assigned to residual carbon from the sample and hydrocarbons from the XPS instrument. The C 1s of *s*-Pani@*m*-TiO_2 shifted to lower BE values in comparison to *s*-Pani@*p*-TiO_2. The Ti 2p was located at a binding energy (BE) of 459.20 ± 0.02 and 464.93 ± 0.02 eV for the *p*-TiO_2 (Fig. S2a) and 459.31 ± 0.02 and 464.99 ± 0.02 eV for the *m*-TiO_2 (Fig. S2b), and were assigned to Ti $2p_{3/2}$ and Ti $2p_{1/2}$ of TiO_2, respectively.[7] The Ti 2p was located at a BE of 459.34 ± 0.02 and 465.16 ± 0.02 eV for the *s*-Pani@*p*-TiO_2 nanocomposite and 458.85 ± 0.02 and 464.59 ± 0.02 eV for the *s*-Pani@*m*-TiO_2 nanocomposite (Fig. 4a), and were assigned to Ti $2p_{3/2}$ and Ti $2p_{1/2}$ of TiO_2, respectively.[7] The BE of Ti $2p_{3/2}$ and Ti $2p_{1/2}$ in the *s*-Pani@*m*-TiO_2 nanocomposite shifted to a lower value (0.49 eV for Ti $2p_{3/2}$ and 0.57 eV for Ti $2p_{1/2}$) compared to the *s*-Pani@*p*-TiO_2 nanocomposite. This lower shift in BE was attributed to the uniform coating of Pani on *m*-TiO_2, which further proves the interfacial interaction between Pani and *m*-TiO_2.

The O 1s peak was located at BE 530.52 ± 0.02 eV and 530.67 ± 0.02 eV for the *p*-TiO_2 (Fig. S2c) and *m*-TiO_2 (Fig. S2d), respectively, and was assigned to the lattice oxygen of TiO_2. The O 1s peak was located at BE 530.58 ± 0.02 eV and 530.07 ± 0.02 eV for the *s*-Pani@*p*-TiO_2 nanocomposite and *s*-Pani@*m*-TiO_2 nanocomposite (Fig. 4b), respectively, and was assigned to the lattice oxygen of TiO_2. The BE of O 1s in the *s*-Pani@*m*-TiO_2 nanocomposite shifted to a lower value (0.51 eV) compared to the *s*-Pani@*p*-TiO_2 nanocomposite. The N 1s peak was located at BE 399.83 ± 0.02 eV and 399.16 ± 0.02 eV for the *s*-Pani@*p*-TiO_2 nanocomposite and *s*-Pani@*m*-TiO_2 nanocomposite (Fig. 4c), respectively, and corresponds to the positive quinoid amine and benzenoid amine present in the Pani structure.[14] The BE of N 1s in the *s*-Pani@*m*-TiO_2 nanocomposite shifted to a lower value (0.67 eV) compared to the *s*-Pani@*p*-TiO_2 nanocomposite. In addition, the Ti 2p, O 1s and N 1s peaks of the *s*-Pani@*m*-TiO_2 nanocomposite were red shifted slightly compared to the *s*-Pani@*p*-TiO_2 nanocomposite. These shifts further confirm the interfacial interaction between Pani and *m*-TiO_2.

Thus it can be concluded that *s*-Pani@*m*-TiO_2 shows shift in the binding energy in comparison to *m*-TiO_2 and *s*-Pani@*p*-TiO_2 which might be due to the interaction between the defective sites of *m*-TiO_2 with Pani. This results in greater lowering of BE in *s*-Pani@*m*-TiO_2 than *m*-TiO_2 and *s*-Pani@*p*-TiO_2. This also supports greater interfacial interaction between the Pani with *m*-TiO_2 than *p*-TiO_2 nanoparticles.[19]

Titanium is a transition metal that has an intense tendency to interact with nitrogen atom in Pani. This interaction may be present in both *s*-Pani@*p*-TiO_2 and *s*-Pani@*m*-TiO_2 nanocomposites.[19] The lower shift in the binding energy of the *s*-Pani@*m*-TiO_2 nanocomposite can be explained by considering the case of elemental nitrogen doping in TiO_2. Nitrogen doping in TiO_2 was reported to shift the binding energy of TiO_2 to a lower binding energy.[20] Because the Pani backbone is rich in nitrogen sites, a possible interaction with the lone pair of nitrogen and defective sites (Ti^{3+} and/or oxygen vacancy) of the *m*-TiO_2 can occur.[21] Therefore, Pani interacts differently with *p*-TiO_2 and *m*-TiO_2 due to the presence of defects, and a much stronger interfacial interaction may exist in the case of the *s*-Pani@*m*-TiO_2 nanocomposite leading to a slight shift in the binding energy. This interfacial interaction may impart novel characteristics to the *s*-Pani@*m*-TiO_2 nanocomposite, which are responsible for the enhanced applications.

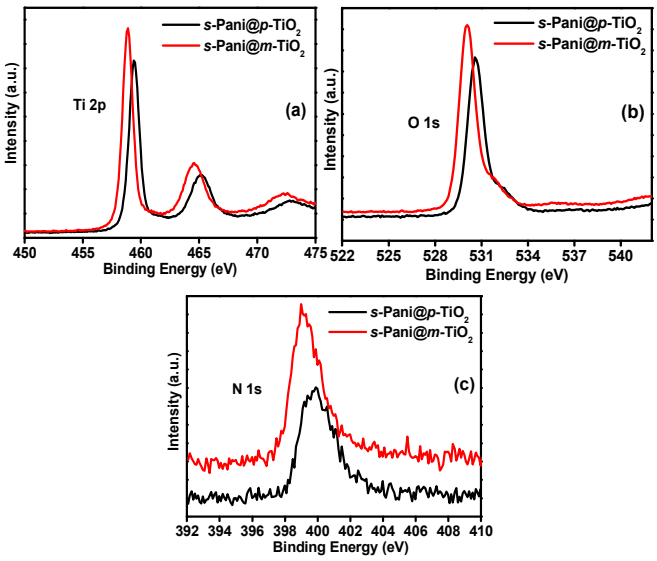

Fig. 4. XP spectra of *s*-Pani@*p*-TiO_2 and *s*-Pani@*m*-TiO_2 nanocomposites for (a) Ti 2p peaks, (b) O 1s peaks, and (c) N 1s peaks.

New Journal of Chemistry Accepted Manuscript

This journal is © The Royal Society of Chemistry 2012

Optical Properties

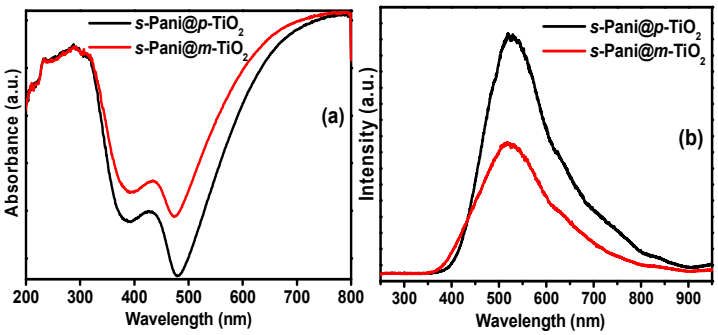

Fig. 5. (**a**) UV-vis diffuse absorbance spectra and (**b**) PL spectra of the *s*-Pani@*p*-TiO_2 and *s*-Pani@*m*-TiO_2 nanocomposites.

Fig. 5a and Fig. S3 shows the UV-vis diffuse absorption and reflectance spectra of the *s*-Pani@*p*-TiO_2 and *s*-Pani@*m*-TiO_2 nanocomposites. *m*-TiO_2 showed higher absorbance in the visible light region compared to *p*-TiO_2, as reported elsewhere.[15] The *s*-Pani@*p*-TiO_2 and *s*-Pani@*m*-TiO_2 nanocomposites showed bands at 280 nm due to a π-π transition in the benzenoid structure, whereas the absorption in the visible range ~400-550 nm was assigned to exciton formation in the quinoid rings. The absorption bands of Pani obtained from the UV-visible absorption spectra were in good agreement with those reported in the literature.[16] After the polymerization of aniline with *p*-TiO_2 and *m*-TiO_2, the resulting *s*-Pani@*p*-TiO_2 and *s*-Pani@*m*-TiO_2 nanocomposite showed greater absorption in the visible light region due to the combinational effect of the narrow band gap of *m*-TiO_2 and the light harvesting/sensitizing property of Pani. This suggests that Pani can be used as a sensitizer, which endows the *s*-Pani@*m*-TiO_2 nanocomposite with visible-light sensitivity.

Photoluminescence (PL) spectroscopy is used widely to study the decrease in the recombination efficiency of the photoinduced electron (e^-) and hole (h^+) pairs of the materials. Emission occurs during the secondary recombination process of photogenerated e^- and h^+ and the intensity is related to the comparative recombination rate. A strong emission intensity means that the photoinduced e^- and h^+ are prone to recombination and the lifetime of the photoinduced e^- and h^+ is short and vice versa.[7] On the other hand, high PL intensities have been reported in the case of *m*-TiO_2 with defects (Ti^{3+} and/or oxygen vacancy) due to the binding property of defects with the photoinduced e^- or h^+ leading to enhanced emission exciton.[15] In this case, the excitation wavelength for both *s*-Pani@*p*-TiO_2 and *s*-Pani@*m*-TiO_2 falls within the visible light region, showing that both are visible light active (Fig. 5b). The peaks in the range, ~475-550 nm, can be assigned to the free electron recombination process from the conduction band (CB) to the ground state recombination center.[7] In contrast to *m*-TiO_2, *s*-Pani@*m*-TiO_2 showed less intense PL peaks compared to *s*-Pani@*p*-TiO_2.[15] Chaturvedi et al.[22] in their bismuth ferrite-Pani core-shell nanoparticles, reported that Pani can also cause oxygen vacancies, local distortions and microstrain in the lattice structures, which greatly affects the optical properties. The microstrain modifies the energy levels, thereby influencing the absorption band edge and hence the change in PL intensity. In the light of this observation, it can be interpreted that due to the preformed defects in *m*-TiO_2, the interaction of Pani with both *m*-TiO_2 and *p*-TiO_2 occurs differently, leading to different levels of local distortion, microstrain and defects. In the light of the above discussion, it can be concluded that Pani decreases the PL intensity, leading to a lower e^--h^+ recombination rate, whereas the defects in *m*-TiO_2 leads to an increase in the PL emission intensity. Therefore, the overall PL peak of *s*-Pani@*m*-TiO_2 is suppressed due to the different type of interfacial interactions between Pani and *m*-TiO_2 or *p*-TiO_2 at the atomic level. Therefore, *s*-Pani@*m*-TiO_2 is expected to have higher photocatalytic activity due to the high level of defects.

DC Electrical Conductivity of *s*-Pani@*p*-TiO_2 and *s*-Pani@*m*-TiO_2 Nanocomposites

The DC electrical conductivity of *s*-Pani@*p*-TiO_2 and *s*-Pani@*m*-TiO_2 nanocomposites were measured using a 4-in-line probe method. The conducting nature of the nanocomposites system can be attributed to the selective interactions between TiO_2 and the quinoid ring of Pani, which facilitates charge transfer from the quinoid ring to TiO_2 via a highly reactive imine group.[23] The DC electrical conductivity of the *s*-Pani@*p*-TiO_2 and *s*-Pani@*m*-TiO_2 nanocomposites were 0.024 and 0.032 S/cm, respectively (Fig. 6). The DC electrical conductivity obtained was much lower than that of the previously reported nanocomposites of Pani with TiO_2.[24] The lower conductivity can be attributed to the small amount of Pani coated on the surface of the TiO_2 nanoparticles due to the dilute polymerization conditions. Other reasons include the electron withdrawing nature of sulfonic groups, which leads to a decrease in the conductivity, as well as to the de-doping phenomenon associated with TiO_2 nanoparticles, which leads to neutralization of the Pani backbone.[16,25] The higher electrical conductivity of the *s*-Pani@*m*-TiO_2 nanocomposite can be attributed to preferential defect formation at the grain boundary sites, which is the major reason for the increase in electrical conductivity.[26] Another reason may be the strong interaction between the nitrogen and Ti^{3+} state of *m*-TiO_2, which provides an alternate pathway for charge transfer. The higher electrical conductivity of the *s*-Pani@*m*-TiO_2 nanocomposite leads to higher electron transfer from the valence band (VB) to the CB, which may also lead to much higher photocatalytic activity and photoelectrochemical performance.

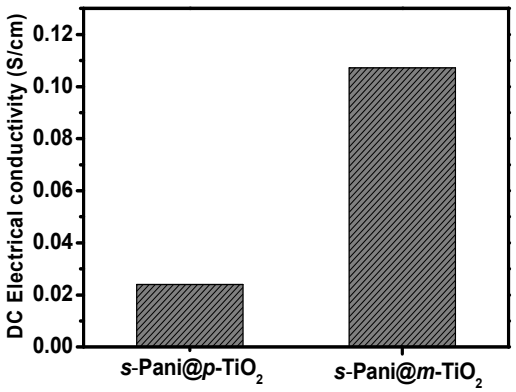

Fig. 6. DC electrical conductivity of the *s*-Pani@*p*-TiO_2 and *s*-

New Journal of Chemistry Accepted Manuscript

Pani@*m*-TiO_2 nanocomposites.

Visible Light Photocatalytic Activities of *s*-Pani@*p*-TiO_2 and *s*-Pani@*m*-TiO_2 Nanocomposites

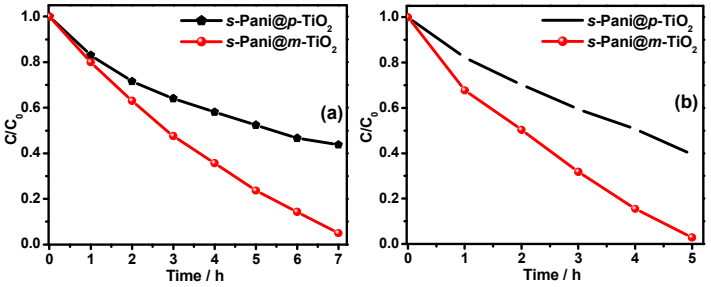

Fig. 7. C/C_0 versus irradiation time (h) plots for the photodegradation of (**a**) MB and (**b**) BB by the *s*-Pani@*p*-TiO_2 and *s*-Pani@*m*-TiO_2 nanocomposites under visible light irradiation.

Photocatalytic degradation experiments were performed to further evaluate the synergistic effect of the sensitization of Pani and the reduced band gap of defective *m*-TiO_2. The photocatalytic degradation efficiency of the *s*-Pani@*p*-TiO_2 and *s*-Pani@*m*-TiO_2 nanocomposites were determined by the photocatalytic degradation of MB and BB dyes under visible light irradiation. The photocatalytic activity of *p*-TiO_2 and *m*-TiO_2 is reported elsewhere.[15] Fig. 7a and 7b show the degradation (C/C_0) as a function of the irradiation time, where C is the absorption of the MB and BB dyes at a given time interval of illumination, and C_0 is the absorption at the initial concentration (time = 0).[5-7] The photocatalytic degradation efficiency of the *s*-Pani@*m*-TiO_2 nanocomposite was significantly higher than that of the *s*-Pani@*p*-TiO_2 as well as *p*-TiO_2 and *m*-TiO_2.[15] Eskizeybek et al.[27] reported the sensitizing effect of Pani for ZnO, giving a high photodegradation efficiency for the degradation of MB and malachite dyes. In view of their observations, Pani may act as photosensitizer for TiO_2 because of its narrower band gap of ~2.81 eV compared to TiO_2.[28] Previous reports also showed that Pani acts as a visible light harvester with high absorption in the visible light region.[7,14] In the case of the *s*-Pani@*p*-TiO_2 nanocomposite, *p*-TiO_2 is not active under visible light irradiation because of its wide band gap (~3.15 eV). Therefore, Pani absorbs visible light and produces an e^- due to the π-π* transition, which is then transferred to the CB of TiO_2 (Fig. 8A). In the case of the *s*-Pani@*m*-TiO_2 nanocomposite, however, *m*-TiO_2 itself absorbs visible light because of its lower band gap of ~2.85 eV, leading to much higher photocatalytic activity than *s*-Pani@*p*-TiO_2.[15] Upon the visible light illumination of *s*-Pani@*m*-TiO_2, the transfer of e^- to the CB of *m*-TiO_2 occurs via a two way process, first by direct transfer from the VB of *m*-TiO_2 and second by the polymer mediated process, i.e. from the lowest unoccupied molecular orbital (LUMO) of Pani (Fig. 8b). This two way e^- transfer leads to the strong accumulation of photogenerated e^- in the CB of *m*-TiO_2. The photoelectrons in the CB of *m*-TiO_2 reacts with the surface adsorbed oxygen to yield superoxide radical anions ($^{\bullet}O_2^-$) and hydroxyl radicals ($^{\bullet}OH$), whereas h^+ reacts with OH^- species to yield $^{\bullet}OH$, which is responsible for the degradation of MB and BB dyes, as shown in Fig. 8B.[29] Another reason for the high photocatalytic activity of *s*-Pani@*m*-TiO_2 is the significantly high separation efficiency of e^--h^+ pairs due to the presence of defects in *m*-TiO_2 comparison to *p*-TiO_2, where these e^--h^+ pairs recombine with each other within a few nanoseconds, resulting in low photocatalytic efficiency.

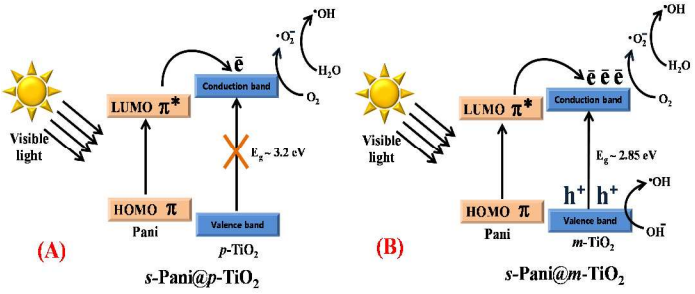

Fig. 8. Proposed mechanism for the photodegradation of MB and BB by the (**A**) *s*-Pani@*p*-TiO_2 and (**B**) *s*-Pani@*m*-TiO_2 nanocomposites under visible light irradiation.

The cyclic stability studies of the *s*-Pani@*m*-TiO_2 photocatalyst after the degradation of the dyes were done by centrifuging, washing and drying the catalyst at 60 ºC. The *s*-Pani@m-TiO_2 photocatalyst showed good recycling ability up to three runs which highlights its reusability (Fig. S4).

Photoelectrochemical Studies

EIS Measurements

The EIS measurements were performed to investigate the electron transfer resistance and charge separation process at the surface of the photoelectrodes. Fig. 9a presents a typical Nyquist plot for the *s*-Pani@*p*-TiO_2 and *s*-Pani@*m*-TiO_2 photoelectrode in the dark and under visible light irradiation. The complex impedance in general is the sum of the real Z' and the imaginary Z'' components, which originate from the resistance and capacitance of the cell, respectively. The Nyquist plot consists of a semicircle on the Z' axis followed by a straight line.[30] The semicircle observed at higher frequencies corresponds to the electron-transfer-limited process, whereas the linear part at lower frequencies represents the diffusion-limited electron-transfer process.[31] In particular, a smaller radius of the arc in the EIS spectra indicates smaller electron transfer resistance at the surface of photoelectrodes, which normally leads to the more effective separation of photogenerated electron-hole pairs and faster interfacial charge transfer.[30,31] In this case, *s*-Pani@*m*-TiO_2 showed a smaller arc radius compared to *s*-Pani@*p*-TiO_2 under visible light irradiation, which indicates the more effective separation of photogenerated electron-hole pairs and faster interfacial charge transfer on the surface of *s*-Pani@*m*-TiO_2. Therefore, the *s*-Pani@*m*-TiO_2 are strongly affected by the photogenerated charge separation, which is related to the synergistic effect of Pani and *m*-TiO_2 (Ti^{3+} formation and/or oxygen vacancies), as explained above. These results are in accordance with the high photocatalytic activity of the *s*-Pani@*m*-TiO_2 nanocomposite. For all the nanocomposites in Fig. 9, the charge transfer resistance is higher under dark conditions than under light conditions. Upon light

New Journal of Chemistry Accepted Manuscript

This journal is © The Royal Society of Chemistry 2012

irradiation, the charge transfer resistance is reduced, mainly due to the emerging of photogenerated charge carriers. These results prove that the Pani deposited onto the *m*-TiO_2 can promote the transfer of photo-generated electrons, inhibiting the recombination of electrons and holes effectively.[32,33]

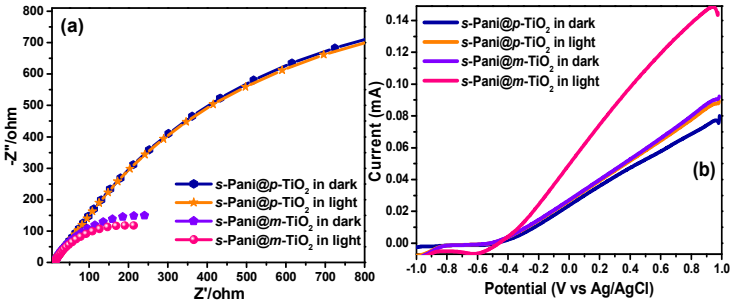

Fig. 9. (a) Nyquist plots and **(b)** LSV obtained for the *s*-Pani@*p*-TiO_2 and *s*-Pani@*m*-TiO_2 in dark and under visible light irradiation.

LSV Measurements

LSV was performed in the dark and under visible light irradiation to further examine the synergistic effect and sensitization ability of Pani and the narrowed band gap of *m*-TiO_2 (Fig. 9b).[34,35] *s*-Pani@*m*-TiO_2 showed a higher photocurrent than *s*-Pani@*p*-TiO_2 under visible light irradiation. The higher photocurrent of *s*-Pani@*m*-TiO_2 was attributed to the higher mobility of charge transfer from Pani to *m*-TiO_2 as well as the transfer of e^- from the VB to CB of *m*-TiO_2 compared to *s*-Pani@*p*-TiO_2, where the transfer of e^- from the VB to CB of *p*-TiO_2 is not feasible due to the wide band gap of *p*-TiO_2. This higher photocurrent displayed by the *s*-Pani@*m*-TiO_2 showed that more photo-induced e^- and h^+ are generated by Pani and defective *m*-TiO_2 (due to the Ti^{3+} formation and/or oxygen vacancies) under visible light irradiation, which explains its high photocatalytic activity under visible light irradiation. Another reason is the effective interfacial interaction between Pani and *m*-TiO_2, which may also contribute to the photoelectron and hole separation, thereby increasing the photocurrent.

Conclusions

s-Pani@*p*-TiO_2 and *s*-Pani@*m*-TiO_2 nanocomposites were prepared by the in-situ oxidative polymerization of aniline in the presence of TiO_2 (*p*-TiO_2 and *m*-TiO_2) nanoparticles. Morphological analysis by HR-TEM showed that a slight coating of Pani formed on the *m*-TiO_2 surface. PL and XPS revealed a strong interaction of Pani via Ti^{3+} and oxygen vacancies in *s*-Pani@*m*-TiO_2 compared to *s*-Pani@*p*-TiO_2. The *s*-Pani@*m*-TiO_2 nanocomposite showed higher DC electrical conductivity and better photoelectrochemical properties because of the higher mobility of charge transfer due to the sensitization ability of Pani and defects in *m*-TiO_2. The *s*-Pani@*m*-TiO_2 nanocomposite showed improved photocatalytic activities in degrading MB and BB compared to *s*-Pani@*p*-TiO_2 under visible light irradiation. The sensitization ability of Pani, presence of defects (Ti^{3+} formation and/or oxygen vacancies) in *m*-TiO_2 and the interfacial interactions between Pani and *m*-TiO_2 were the main reasons for the enhanced visible light photocatalytic activity and photoelectrochemical properties. These defects can facilitate the separation of photogenerated electron-hole pairs and increase the photocatalytic activity and photoelectrochemical performance, such as EIS and LSV. In addition, the effective interfacial interaction between Pani and *m*-TiO_2, which may also contribute to photoelectron and hole separation, enhanced the visible light induced photoactivities of the as-prepared *s*-Pani@*m*-TiO_2 nanocomposite. The proposed methodology of using EB irradiation and conducting Pani for the band gap tuning of nanocomposites for visible light application provides an alternate and much greener route for the development of new and highly efficient photocatalyst materials.

Acknowledgements

This study was supported by Priority Research Centers Program (Grant No:2014R1A6A1031189), and by Basic Science Research Program (Grant No:2015R1D1A3A03018029) through the National Research Foundation of Korea (NRF) funded by the Ministry of Education.

Notes and references

[a]*School of Chemical Engineering, Yeungnam University, Gyeongsan-si, Gyeongbuk 712-749, South Korea. Phone: +82-53-810-2517; Fax: +82-53-810-4631.*
[b]*Chemical Sciences, Faculty of Science, Universiti Brunei Darussalam, Jalan Tungku Link, BE 1410, Brunei Darussalam.*
Corresponding authors
***Email:** mhcho@ynu.ac.kr; omaishchem@gmail.com; mmansoobkhan@yahoo.com*

†Electronic Supplementary Information (ESI) available: [XPS survey, C 1s and UV-vis diffuse reflectance spectra of *s*-Pani@*p*-TiO_2; *s*-Pani@*m*-TiO_2 nanocomposites stability spectra, Ti 2p and O 1s spectra of *p*-TiO_2 and *m*-TiO_2] See DOI: 10.1039/b000000x/

1 A. Fujishima, K. Honda, *Nature* 1972, **238**, 37–38.
2 K. Nakata, A. Fujishima, *J. Photochem. Photobiol.* C 2012, **13 (3)**, 169−189.
3 S. G. Kumar, L. G. Devi, *J. Phys. Chem. A* 2011, **115**, 13211−13241.
4 K. Sayama, S. Tsukagoshi, K. Hara, Y. Ohga, A. Shinpou, Y. Abe, S. Suga, H. Arakawa, *J. Phys. Chem. B* 2002, **106**, 1363−1371.
5 S. Liu, E. Guo, L. Yin, *J. Mater. Chem.* 2012, **22**, 5031−5041.
6 M. M. Khan, S. A. Ansari, O. M. Ansari, B. K. Min, J. Lee, M. H. Cho, *J. Phys. Chem. C* 2014, **118**, 9477−9484.
7 M. O. Ansari, M. M. Khan, S. A. Ansari, K. Raju, J. Lee, M. H. Cho, *ACS Appl. Mater. Interfaces* 2014, **6**, 8124−8133.
8 M. J. Kim, K. D. Kim, W. S. Tai, H. O. Seo, Y. Luo, Y. D. Kim, B. C. Lee, O. K. Park, *Catal. Lett.* 2010, **135**, 57–61.

New Journal of Chemistry Accepted Manuscript

9 X. Pan, M.-Q. Yang, X. Fu, N. Zhang, Y.-J. Xu, *Nanoscale* 2013, **5**, 3601−3614.
10 X. G. Hou, A. D. Liu *Radiat. Phys. Chem.* 2008, **77**, 345–351.
11 X. G. Hou, X. N. Gu, Y. Hu, J. F. Zhang, A. D. Liu, *Nucl. Instrum. Meth. B* 2006, **251**, 429–434.
12 J. Jun, M. Dhayal, J. H. Shin, J. C. Kim, N. Getoff, *Radiat. Phys. Chem.* 2006, **75**, 583–589.
13 H. O. Seo, C. W. Sim, K. D. Kim, Y. D. Kim, J. H. Park, B. C. Lee, K. H. Lee, D. C. Lim, *Radiat. Phys. Chem.* 2012, **81**, 290–294.
14 M. O. Ansari, M. M. Khan, S. A. Ansari, J. Lee, M. H. Cho, *RSC Adv.* **2014**, 4, 23713–23719.
15 M. M. Khan, S. A. Ansari, D. Pradhan, M. O. Ansari, D. H. Han, J. Lee, M. H. Cho, *J. Mater. Chem. A* 2014, **2**, 637−644.
16 M. O. Ansari, M. M. Khan, S. A. Ansari, I. Amal, J. Lee, M. H. Cho, *Mater. Lett.* 2014, **114**, 159–162.
17 X. Wang, J. X. Deng, X. J. Duan, D. Liu, J. S. Guo, P. Liu, *J. Mater. Chem. A* 2014, **2**, 12323–12329.
18 K. P. Priyanka, N. A. Sabu, A. T. Sunny, P. A. Sheena, T. Varghese, *Journal of Nanotechnology*, 2013, **2013**, Article ID 580308, 6 pages.
19 M. R. Nabid, M. Golbabaee, A. B. Moghaddam, R. Dinarvand, R. Sedghi, *Int. Electrochem. Sci.* 2008, **3**, 1117–1126.
20 Y. Liu, K. Mu, G. Yang, H. Peng, F. Shen, L. Wang, S. Deng, X. Zhang, Y. Zhang, *New J. Chem.* 2015, DOI: 10.1039/C5NJ00340G.
21 S. Wei, P. Mavinakuli, Q. Wang, D. Chen, R. Asapu, Y. Mao, N. Haldolaarachchige, D. P. Young, Z. Guo, *J. Electrochem. Soc.* 2011, **158**, K205−K212.
22 S. Chaturvedi, R. Das, P. Poddar, S. Kulkarnia, *RSC Adv.* 2015, **5**, 23563–23568.
23 S. Ameen, M. S. Akhtar, Y. S. Kim, H. S. Shin, *Prof. Leonid A. Kosyachenko (Ed.)*, 2011, ISBN: 978-953-307-735-2, InTech, DOI: 10.5772/19889.
24 M. O. Ansari, F. Mohammad, *Sens. Actuators, B*, 2011, **157**, 122–129.
25 M. O. Ansari, F. Mohammad, *J. Appl. Polym. Sci.* 2012, **124**, 4433–4442.
26 S. A. Ansari, M. M. Khan, M. O. Ansari, S. Kalathil, J. Lee, M. H. Cho, *RSC Adv.* 2014, **4**, 16782−16791.
27 V. Eskizeybek, F. Sari, H. Gulce, *Appl. Catal., B* 2012, **119**, 197−206.
28 S. X. Xiong, Q. Wang, H. S. Xia, *Synth. Met.* 2004, **146**, 37−42.
29 Z. Khan, T. R. Chetia, A. K. Vardhaman, D. Barpuzary, C. V. Sastri, M. Qureshi, *RSC Adv.* 2012, **2**, 12122–12128.
30 L. Zhao, L. Fang, W. Dong, F. G. Zheng, M. R. Shen, *Appl. Phys. Lett.* 2013, **102**, 121905-5.
31 W. H. Leng, Z. Zhang, J. Q. Zhang, C. N. Cao, *J. Phys. Chem. B* 2005, **109**, 15008–15023.
32 N. Li, S. Jayaraman, S. Y. Tee, P. S. Kumar, C. J. J. Lee, S. L. Liew, D. Chi, T. S. A. Hor, S. Ramakrishna, H.-K. Luo, J. Mater. Chem. A, 2014,2, 19290-19297.
33 W. Teng, X. Li, Q. Zhao, G. Chen, J. Mater. Chem. A, 2013,1, 9060-9068.
34 J. Gan, X. Lu, J. Wu, S. Xie, T. Zhai, M. Yu, Z. Zhang, Y. Mao, S. C. Wang, Y. Shen, Y. Tong, *Sci. Rep.* 2013, **3**, 1021–1028.
35 S. A. Ansari, M. M. Khan, M. O. Ansari, M. H. Cho, Solar Energy Materials & Solar Cells 2015, 1**41**, 162−170.

New Journal of Chemistry Accepted Manuscript

This journal is © The Royal Society of Chemistry 2012